

Electronic Supplementary Information

Largely enhanced mechanical performance of poly(butylene succinate) multiple system via shear stress-induced orientation of hierarchical structure

Xu-Long Xie, Yue Li, Jia-Zhuang Xu, Zheng Yan, Gan-Ji Zhong*, Zhong-Ming Li
College of Polymer Science and Engineering, State Key Laboratory of Polymer
Materials Engineering, Sichuan University, Chengdu, 610065, China

***Corresponding Author:**

*Phone: +86-28-8540-0211. Fax: +86-28-8540-6866.

E-mail: ganji.zhong@scu.edu.cn. (G.-J.Z.).

1. The feature of oscillation shear injection molding (OSIM)

Fig. S1 shows the digital photograph of OSIM machine. For OSIM processing, melt is first injected into the mold cavity after the preplasticizing stage, which is similar with conventional injection molding (CIM). Differently, the mold was equipped with an oscillation shear supplier, as shown in Fig. S2.^{1,2} To be clear, schematic illustration of the special mold is shown in Fig. S3.³ The two pistons equipped on the mold part move out of phase and make the polymer melt periodically move in the length direction of moldings during packing stage. The shear flow of melt takes place until the gate is solidified. In other words, before being frozen, the melt continuously undergoes repeated shear stress, unless the pistons are stopped. As a result of this, the sufficiently high shear rate (over 1000 s^{-1}) can impose on the melt in interior region with the increase of the thickness of solidified layer. In this way, oriented hierarchical structure can be controlled in the both skin and inner layers of OSIM parts. For CIM parts, the oriented hierarchical structure can be obtained only in the very narrow region near the mold wall.^{4,5} The mechanical properties of the OSIM parts can be measured by common measurement such as tensile testing and notched Izod impact test. Therefore, OSIM technology is also a powerful tool to establish relationship between oriented hierarchical structure and performances.



Fig. S1. Digital photograph showing the OSIM machine

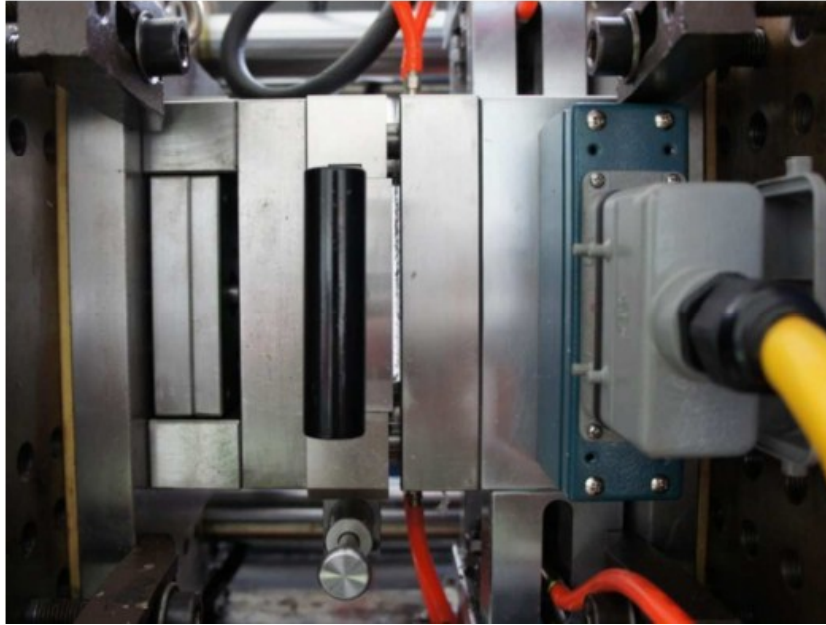


Fig. S2. Local picture for the mold with an oscillation shear supplier.

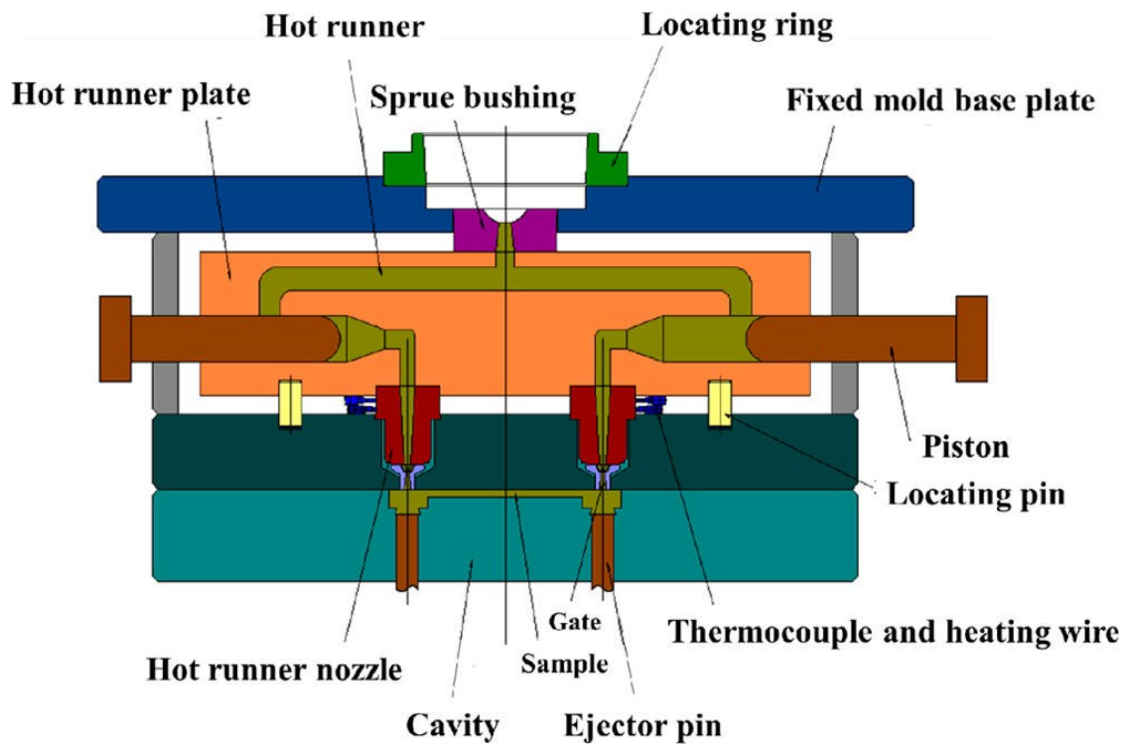


Fig. S3. Schematic illustration of OSIM mold.

2. Semi-quantitative shear rate and temperature distribution during OSIM processing

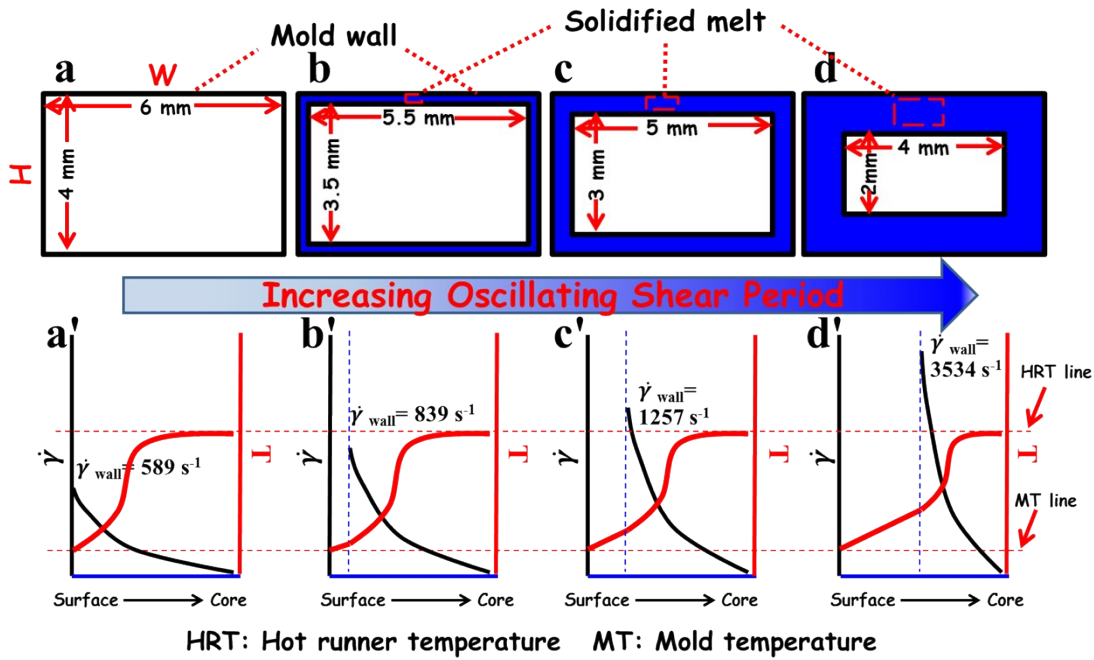


Fig. S4 Schematic depiction of the proposed conceptual model. Oscillating shear period increases from left to right. Top row shows morphology at a cross-section vertical to the flow direction in the mold, bottom row shows shear rate and temperature versus position from skin to core layers.

The following conceptual model is proposed to illustrate shear rate and temperature distribution during OSIM processing and explain the experimental observations presented in this paper.⁶⁻⁸ Fig. S4 illustrates the profile of shear rate and temperature in cavity during OSIM processing, which is helpful for explanation of the results obtained. Figs S5 a-d show schematic depiction of the view at cross-section vertical to the flow direction during solidification in the mold cavity in the top row. Figs S4 a'-d' in the bottom row show the profile of shear rate and temperature versus position from skin to core layers. Oscillation shear duration increases from left to right. With oscillation shear duration, the thickness of solidified layer increases because of a low mold temperature (40 °C). The shear rate near the walls can be calculated from Equation S1. The shear rate from skin to core is shown in bottom row with black line. Shortly after the start of flow, a flow profile develops with the maximum of shear rate near solidified line and zero at the center of the mold cavity (Fig. S4 a'-d'). Because the total volumetric flow

rate remains constant, the maximum of shear rate experienced by the polymer melt at the solidified line increases. The red lines in the bottom row represent the temperature profile of polymer matrix from the solidified part to just solidified part then to the core part. The hot runner temperature in this work is 140 °C, so the temperature in the core layer of part is thought to be 140 °C. The temperature of solidified layer is near the mold temperature, and increases with the thickness of solidified layer, due to the poor heat transferring ability of polymer and the high temperature in the core layer. The temperature has a large impact on the relaxation of stretched chain. The stretched chains near the solidified layer can be inhibited from relaxation and remain to develop into aligned lamellae precursor. As a result, flow-induced aligned lamellae precursor near the wall leads to aligned lamellae with high density, and its density quickly falls off from the wall to the center of the mold cavity. This sequence of events continues until flow is ceased.

$$\dot{\gamma} = \frac{6q_v}{Wh^2} \dots \dots \dots \text{(Equation 1)}$$

where q_v represents the volumetric flow rate ($3\pi \text{ cm}^3/\text{s}$), W and h are the width (6mm) and thickness (4mm) of cross section, respectively.

3. Comparison of complex viscosity of PBS and PBS/PLA blends

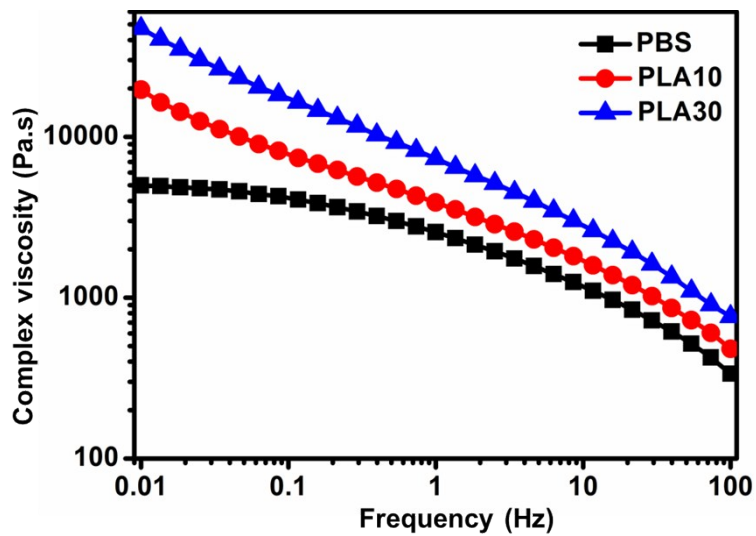


Fig. S5. Comparison of complex viscosity of PBS and PBS/PLA blends at 120 °C.

The addition of 30 wt% PLA makes the viscosity of melt very large (see Figure S5), thus, the gate is solidified in a shorter time compared with PBS and PLA10. In this way the period of effective oscillation shear flow imposed on PLA30 is less than others, so the thickness of shish-kebab layer is decreased to about 500 μm .

4. Crystallinity of PBS and PLA in neat PBS and PBS/PLA blends

Table S1. Crystallinity of PBS in neat PBS and PBS/PLA blends by OSIM and CIM processing at different regions away from the surface

Samples	positions (distance away from surface, μm)				
	100	500	1000	1500	2000
PBS-CIM	0.22	0.28	0.27	0.28	0.31
PBS-OSIM	0.20	0.29	0.24	0.28	0.33
PLA10-CIM	0.23	0.29	0.28	0.29	0.32
PLA10-OSIM	0.24	0.28	0.27	0.27	0.31
PLA30-CIM	0.24	0.31	0.31	0.31	0.32
PLA30-OSIM	0.22	0.31	0.32	0.33	0.34

The crystallinity of PBS has a large impact on the mechanical performance since its glass transition temperature is below zero degree and PBS is the matrix in the blend.⁹⁻
¹¹ Therefore, the crystallinity of PBS in the samples was estimated by a standard peak-fitting procedure of the WAXD intensity profile. The calculated crystallinity of PBS shown in Table S1 indicates that all the samples have similar crystallinity distribution between CIM and OSIM samples. The crystallinity of PBS at the skin region is lower compared with the inner region, due to the larger cooling rate of melt contacting with the mold wall. The crystallinity of PBS increases with the distance from the surface increasing. The melt in the inner layers has a lower cooling rate, thus provides more time to crystallization or complete crystal. In addition, blending PLA hardly affects the crystallinity of PBS. The average crystallinity of PBS increases slightly from 28% to 32% with the content of PLA 30 wt%, which is infer to result from promoting effect by 30 wt% PLA. This phenomenon is consistent with the SAXS results that 30wt% PLA

has hardly impact on d_c , but decrease d_a . However, the mechanism is unclear now and will be studied in our further work.

Table S2. Crystallinity of PLA in PBS/PLA blends by OSIM and CIM processing at different regions away from the surface

Samples	positions (distance away from surface, μm)				
	0	500	1000	1500	2000
PLA10-CIM	0.03	0.08	0.22	0.04	0.00
PLA10-OSIM	0.15	0.19	0.17	0.08	0.11
PLA30-CIM	0.11	0.04	0.09	0.00	0.00
PLA30-OSIM	0.03	0.07	0.00	0.00	0.00

Crystallinity of PLA in PBS/PLA blends by OSIM and CIM processing at different regions away from the surface is shown in Table S2. For CIM PLA 10 and PLA30, the crystallinity of PLA is low, due to the high cooling rate and low crystallization kinetics. However, at intermediate layer 1000 μm away from the surface, the crystallinity is high, because of shear – induced crystallization and proper cooling rate. At core layer, the crystallinity of PLA decreases to zero, because of oriented chain relaxation during cooling. For OSIM PLA10, the crystallinity of PLA from skin to core layers is similar and ranges 0.08 ~ 0.19, due to the oscillation shear during cooling. However, for OSIM PLA30, the crystallinity is very low. We conjectured that the addition of 30 wt% PLA makes the viscosity dense, thus, the polymer chain being stretched becomes difficult.

5. The inner morphologies of neat PBS and PBS/PLA blend parts

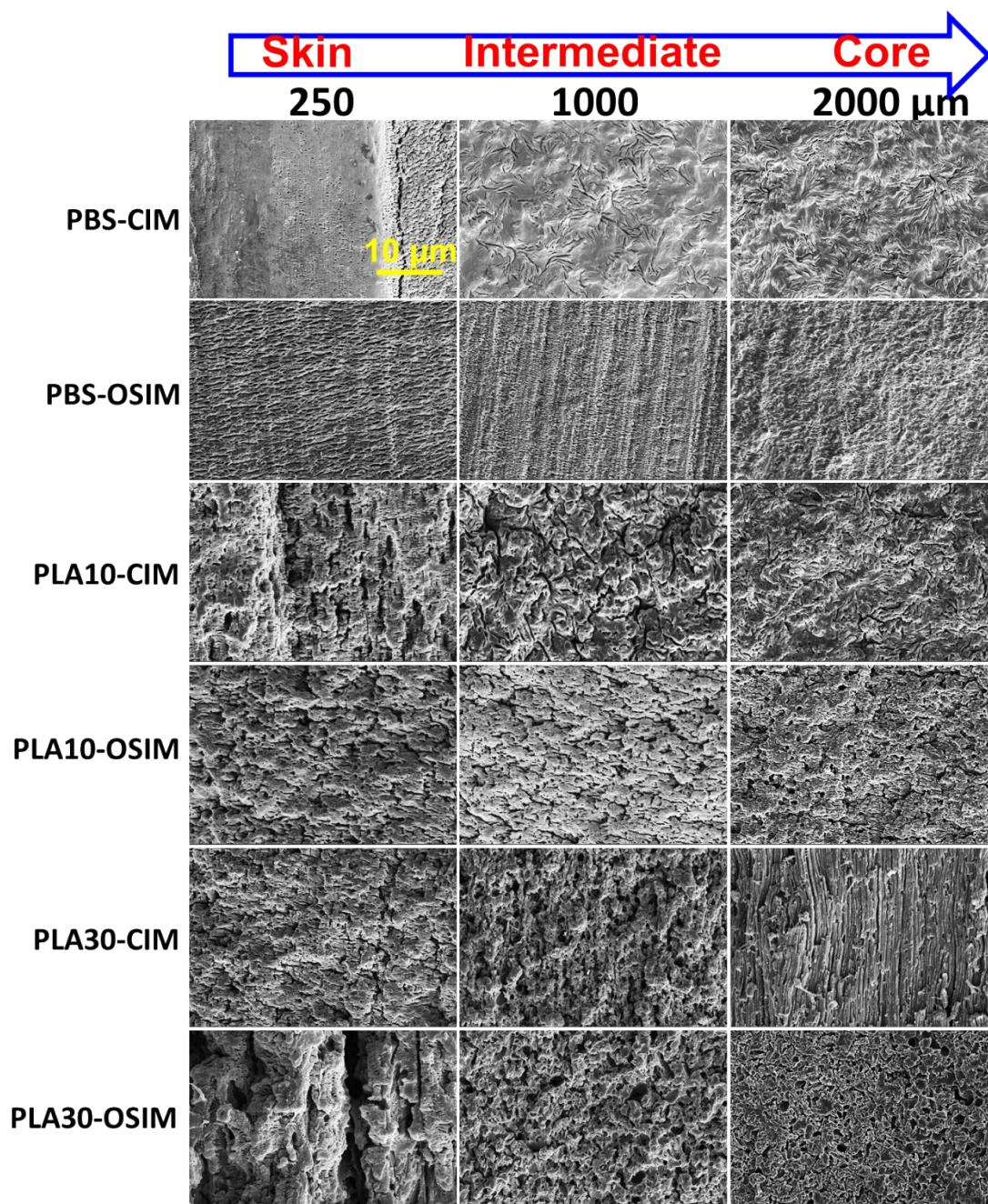


Fig. S6. The less magnified picture of the crystalline morphology and its distribution in PBS and PBS/PLA blends by CIM and OSIM.

Figure S6 shows many shish-kebabs and spherulites formed in the samples with a less magnification. The neighboring shish-kebabs are interlocked with each other, that is, a lamella in a shish-kebab may grow into the space between two lamellae of another adjoining shish-kebab. The spherulites are quite typical.

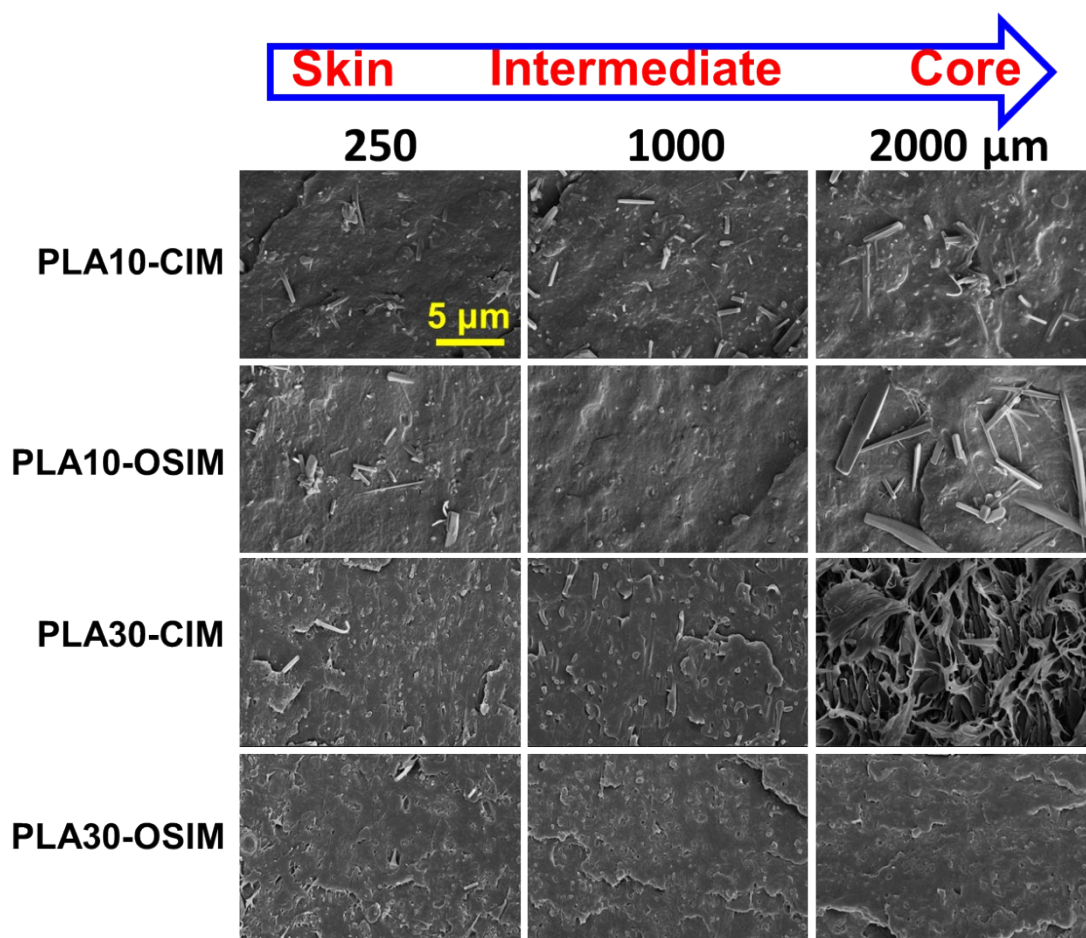


Fig. S7. Representative SEM micrographs revealing phase morphology of PBS/PLA blends by OSIM and CIM processing at different regions away from the surface.

The phase morphology of the PBS/PLA blends by OSIM and CIM processing at different regions away from the surface is shown in Figure S7. The microfibrillar morphology of dispersed PLA phase was formed. The microfibrillation occurs in melting with screws rotating and mold filling, during which intense shearing and stretching flow field is inevitable. The shearing and stretching effect on PBS/PLA blend melt facilitates deformation of PLA within PBS by extension of the molecular chains. The processing temperature is set just at the initial melting temperature of PLA, prolonging the breakup time of the dispersed fibrous phase of PLA. Notably, a co-continuous structure likely formed in CIM PLA30, from which we infer the ununiformed distribution of dispersed PLA phase. As was provided Figure S5, blending 30wt% PLA into the PBS matrix makes the viscosity much higher compared with neat

PBS. It is inferred that the PBS matrix of CIM PLA30 with low viscosity intends to disperse in out layer and the dispersed PLA with high viscosity intends to be in inner layer. Therefore, the content of PLA in core layer is larger than 30wt%, and reach the critical content of forming co-continuous structure. However, for OSIM PLA30, less PLA microfiber is found from skin to core layer. Therefore, breaking up of the dispersed fibrous phase of PLA may occur during melt flowing in hot runner where melt suffers both shear flow and high temperature resulted from hot runner and shear-induced heat.

6. Thermal mechanical properties of injection-molded neat PBS and PBS/PLA blends

The dynamic mechanical properties were measured on a DMA Q800 (TA Instruments, USA) in a multifrequency strain mode with a dual cantilever clamp (the ASTM standard D4065) at a frequency of 1 Hz. The amplitude was set as 15 μm within the linear viscoelastic region. The sample with the dimension $60 \times 6 \times 4 \text{ mm}^3$ was heated from 30 to 110 $^{\circ}\text{C}$ at a heating rate of 3 $^{\circ}\text{C}/\text{min}$.

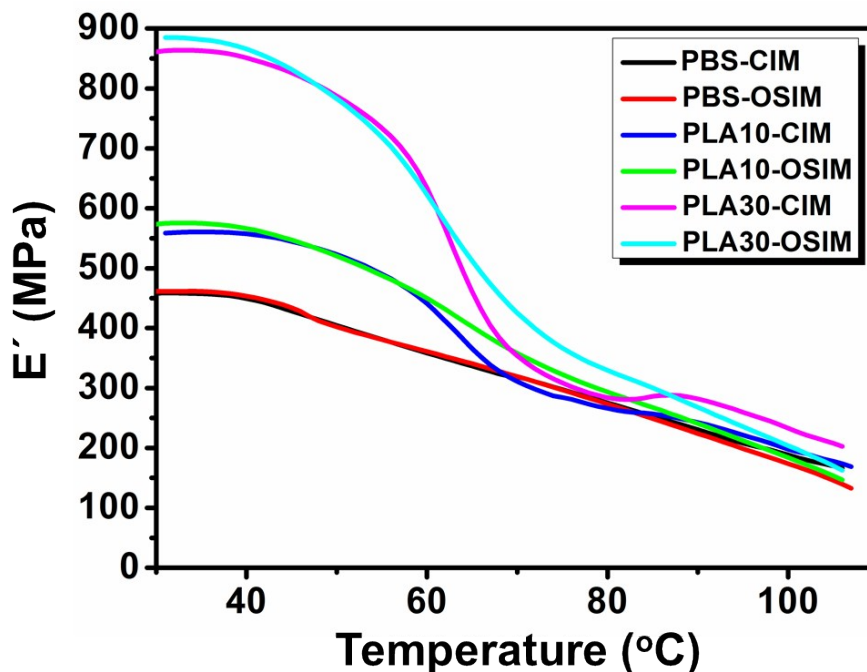


Fig. S8. Temperature dependence of storage modulus of neat PBS and PBS/PLA blends by OSIM and CIM processing, obtained from DMA.

Figure S8 illustrates temperature dependence of the storage modulus of neat PBS and PBS/PLA blends by OSIM and CIM processing. Expectedly, the E' value of composites monotonically increased with the content of PLA increasing especially at room temperature. This improvement was due to the reinforcing effect of PLA in the PBS matrix, which allows stress transfer from the PBS to PLA. In addition, the E' values of OSIM samples are similar with corresponding CIM samples. Tensile modulus mentioned in former section and storage modulus is quite different. Tensile modulus is obtained by stretching the samples; while, storage modulus is obtained by bending the samples in this work. Therefore, shish-kebab structure hardly changes the bending modulus in contrast to the spherulite structure in PBS based materials. The values of the storage modulus observed at 35°C (room temperature), and at 80°C (higher temperature) are shown in Table S3. We can see that the addition of PLA improves the stiffness of PBS at room temperature, and has slight positive effect on the stiffness at higher temperature, obviously, which is beneficial for the wide application of PBS.

Table S3. Storage modulus of neat PBS and PBS/PLA blends by OSIM and CIM processing at 35 and 100 °C.

Samples	E'(35°C)/MPa		E'(80°C)/MPa	
	CIM	OSIM	CIM	OSIM
PBS	458	461	275	273
PLA10	560	575	266	294
PLA30	863	882	284	330

7. The crystalline structure of samples after tensile deformation by 2D-WAXD and 2D-SAXS

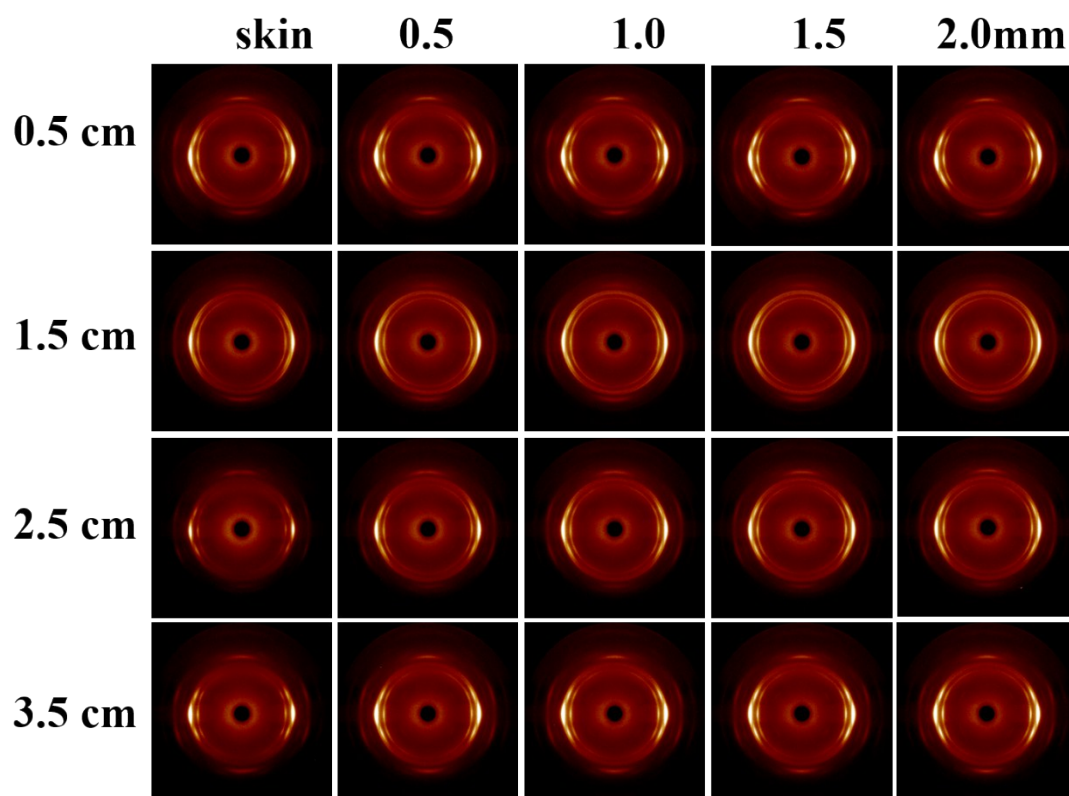


Fig. S9. 2D-WAXD patterns of stretched OSIM PBS at different regions away from the skin. The labels of 0.5 cm, 1.5 cm, 2.5 cm and 3.5 cm represent the positions away from the breaking point along the length direction. The shear flow direction is vertical.

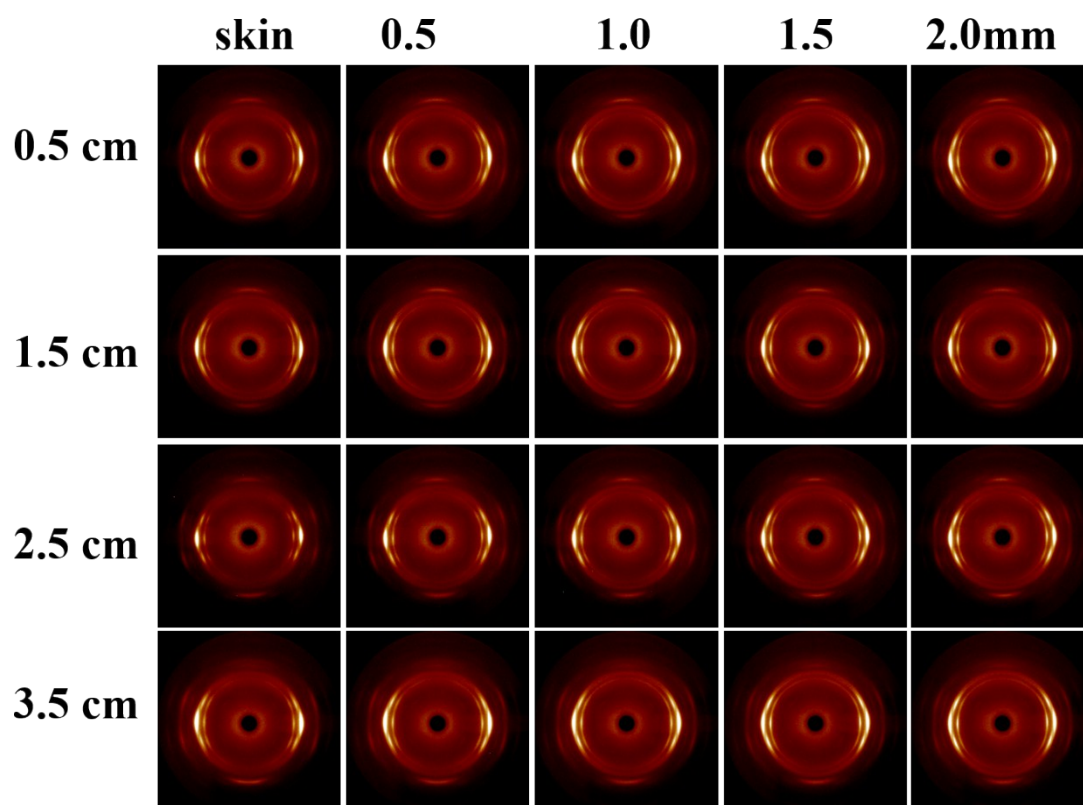


Fig. S10. 2D-WAXD patterns of stretched CIM PBS at different regions away from the skin. The labels of 0.5 cm, 1.5 cm, 2.5 cm and 3.5 cm represent the positions away from the breaking point along the length direction. The shear flow direction is vertical. As shown in Figure S9 and S10, highly oriented chain segments form after tensile testing. In addition, there is hardly difference in the 2D-WAXD patterns of selected points from skin to core layers and 0.5 cm, 1.5 cm, 2.5 cm and 3.5 cm away from the breaking point along the length direction. This indicates a homogenous and oriented structure forms in OSIM and CIM samples after tensile testing.

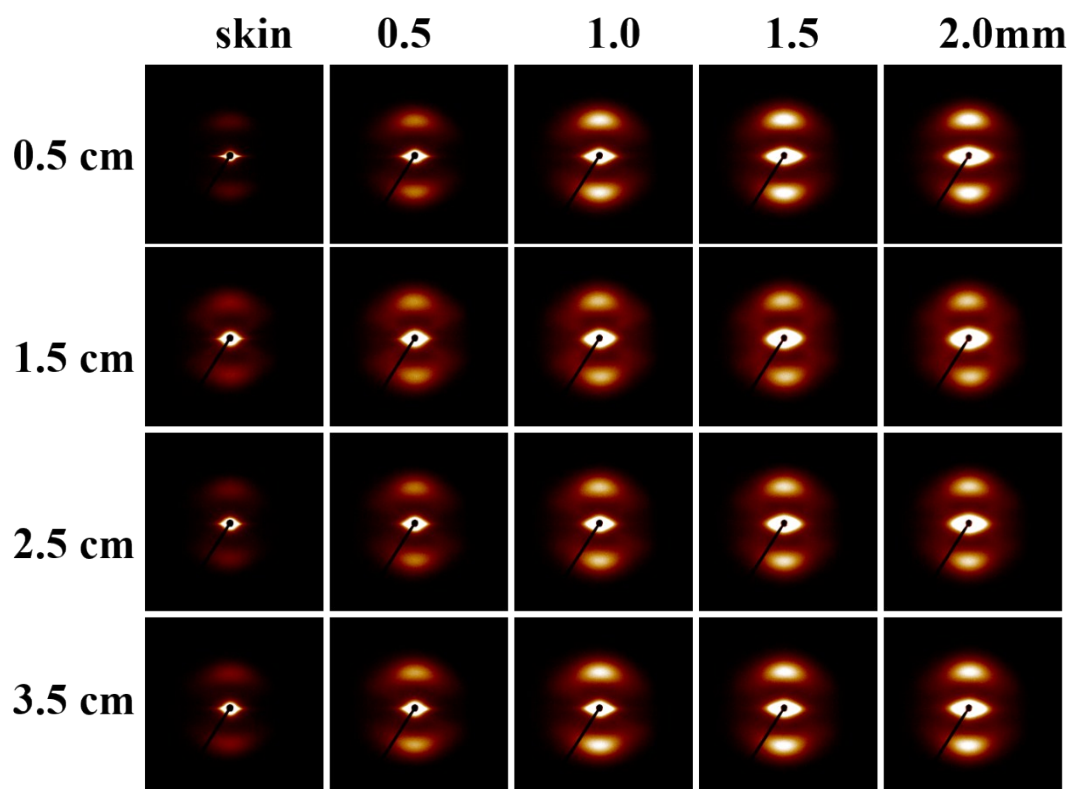


Fig. S11. 2D-SAXS patterns of stretched OSIM PBS at different regions away from the skin. The labels of 0.5 cm, 1.5 cm, 2.5 cm and 3.5 cm represent the positions away from the breaking point along the length direction. The shear flow direction is vertical.

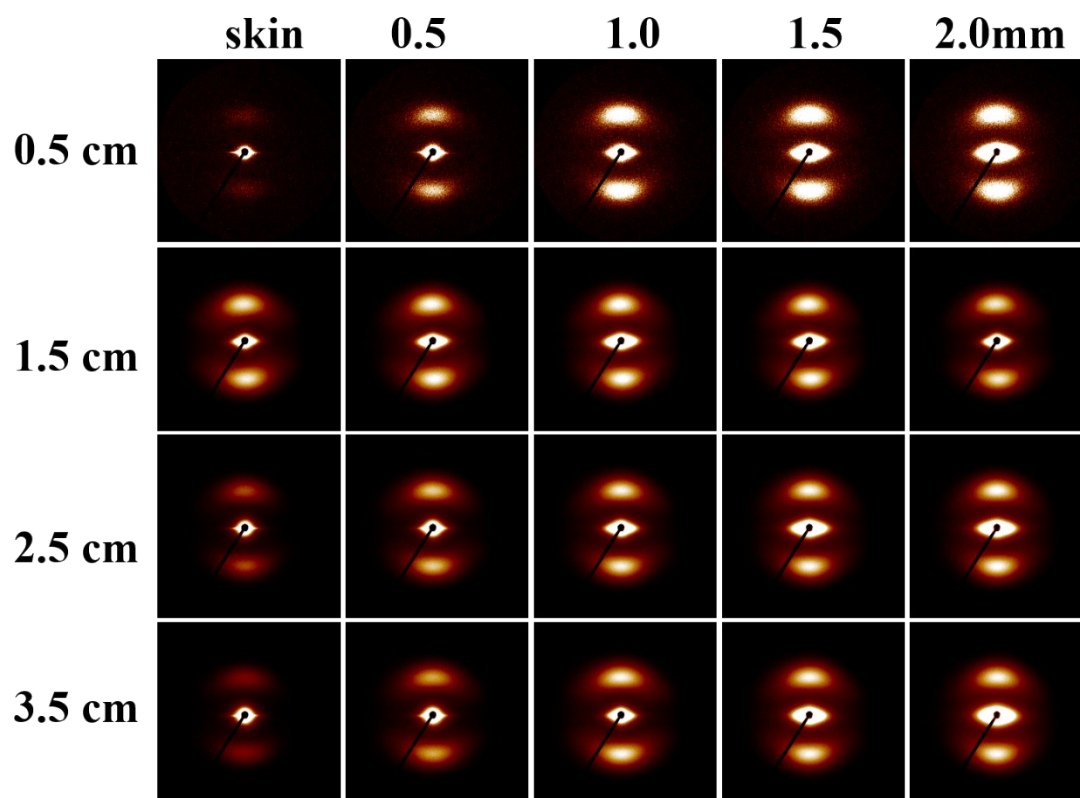


Fig. S12. 2D-SAXS patterns of stretched CIM PBS at different regions away from the skin. The labels of 0.5 cm, 1.5 cm, 2.5 cm and 3.5 cm represent the positions away from the breaking point along the length direction. The shear flow direction is vertical.

As shown in Figure S11 and S12, highly oriented lamellae form after tensile testing. In addition, there is hardly difference in the 2D-SAXS patterns of selected points 0.5 cm, 1.5 cm, 2.5 cm and 3.5 cm away from the breaking point along the length direction. However, the intensity of X-ray scattering at low q values increase from skin to core, especially from OSIM PBS. The increase of X-ray scattering at low q values is indicative of forming cavity. There are two possibilities. First, the distribution of stress from skin to layer is inhomogeneous, thus resulting in the difference of cavity distribution. Second, the denser and higher oriented structure of out layers from intense shear stress produces less cavity than lower oriented structure of the inner layers during the tensile deformation.

References

1. H. Xu, L. Xie, Y.-H. Chen, H.-D. Huang, J.-Z. Xu, G.-J. Zhong, B. S. Hsiao, Z.-M. Li, *ACS Sustain. Chem. Eng.*, 2013, **1**, 1619-1629.
2. H. Xu, G.-J. Zhong, Q. Fu, J. Lei, W. Jiang, B. S. Hsiao, Z.-M. Li, *ACS Appl. Mater. Interfaces*, 2012, **4**, 6773-6783.
3. Z. Zhang, R. Zhang, Y. Huang, J. Lei, Y. -H. Chen, J. -H. Tang, Z. -M. Li, *Ind. Eng. Chem. Res.*, 2014, **53**, 10144-10154.
4. G.-J. Zhong, Z. -M. Li, *Polym. Eng. Sci.*, 2005, **45**, 1655-1665
5. K. Wang, F. Chen, Z. Li, Q. Fu, *Prog. Polym. Sci.*, 2014, **39**, 891-920.
6. X.-L. Xie, Q.-S. Sun, J. Lei, F. Tian, L. Xu, Z. Yan, G.-J. Zhong, Z.-M. Li, *J. Mater. Chem. A*, 2017, **5**, 22697-22707.
7. P. C. Roozmond, M. van Drongelen, Z. Ma, A. B. Spoelstra, D. Hermida-Merino, G. W. Peters, *Macromol. Rapid Commun.*, 2015, **36**, 385-390.
8. Y. Pan, S. Shi, W. Xu, G. Zheng, K. Dai, C. Liu, J. Chen, C. Shen, *J. Mater. Sci.*, 2014, **49**, 1041-1048.
9. T. X. Jin, M. Zhou, S.-D Hu, F. Chen, Q. Fu, Y. Fu, *Chinese J. Polym. Sci.*, 2014,

32, 953-960.

10. B. Yang, H. Ni, J. Huang, Y. Luo, *Macromolecules*, 2014, **47**, 284-296.

11. T. Dong, K. M. Shin, B. Zhu, Y. Inoue, *Macromolecules*, 2006, **39**, 2427-2428.